Ground-state properties of microcavity polariton condensates at arbitrary excitation density

Kenji Kamide* and Tetsuo Ogawa
Department of Physics, Osaka University, Toyonaka, Osaka 560-0043, Japan
(Received 5 October 2010; revised manuscript received 4 February 2011; published 25 April 2011)

The ground state of microcavity polariton Bose-Einstein condensates (BEC's) is determined as a function of experimentally tunable parameters (the excitation density and the detuning of cavity photons), and also a material parameter (the ultraviolet cutoff). To obtain the ground state at an arbitrary excitation density, an interpolation method for the BEC-BCS crossover of excitonic insulators is extended to microcavity polariton systems in two or three dimensions. The ground state of the condensate changes from excitonic to photonic with an increase in the excitation density. This change is accompanied by several interesting features: (i) A laserlike input (excitation density) and output (photon density) relation with a sharp onset for largely detuned systems, which changes to that with a smooth onset for slightly detuned systems. (ii) The origin of the binding force of electron-hole pairs changes from Coulomb attraction to photon-mediated interactions, resulting in the formation of strongly bound pairs with a small radius, such as Frenkel excitons, in the photonic regime. The change in the ground state can be a crossover or a first-order transition, depending on the above-mentioned parameters, and is studied by plotting phase diagrams.

DOI: 10.1103/PhysRevB.83.165319 PACS number(s): 71.36.+c, 71.35.Lk, 73.21.−b, 03.75.Hh

I. INTRODUCTION

Polaritons in semiconductor microcavities have been observed to exhibit Bose-Einstein condensation (BEC).[1,2] Because of light-matter coupling, the polariton has an extremely small mass (10^{-4} times the free-electron mass), resulting in a high critical temperature and low critical density. The transition temperature of polariton condensation can be higher than room temperature,[3] which is remarkable considering that it has been difficult to realize BEC in exciton systems for a long time.[4] This implies that polariton condensates are robust against fluctuations once they achieve quantum coherence. In fact, in many ways, a polariton BEC is similar to a BEC of neutral atoms in a thermal equilibrium,[5] despite its nonequilibrium nature. A great deal of evidence has been obtained for the superfluidity of polariton condensates, such as the detection of the Goldstone mode[6] and quantized vortices,[7] by measuring their collective fluid dynamics[8] and Landau critical velocity.[9]

All the above experiments have been carried out in a low-density regime where excitons can be regarded as bosons (for a recent review article, see Ref. 10). In the high-density regime, the dissipative nature of polaritons dominates and normal lasing occurs due to the carrier heating.[11,12] The threshold density of lasing is much higher than that of BEC. Therefore, in the current experimental situations, polariton systems can be regarded as ground states at low density and nonequilibrium stationary-state like lasers at high density. In both cases, however, polariton condensates are in a nonequilibrium stationary state with a balance between pumping and losses.[13–15] Which situation occurs depends on two time scales, i.e., the lifetime of the polaritons and the thermalization time.[14,16] Although not observed in the current experiments, the possibility of quantum condensation of polaritons at high density cannot be ruled out. Such condensates formed at high density may differ from the conventional lasers[17] and the polariton condensates formed at low density. Therefore, the relationship between a polariton BEC at high density and lasers will have to be clarified. To this end, here, we study the ground states of polariton condensates at an arbitrary excitation density. We have recently reported the main results in a Brief Report[18] for this problem. In this paper, more detailed results and a detailed comparison to other related systems, such as electron-hole systems without cavity and lasers, are shown.

When the polariton lifetime is longer than the thermalization time, the stationary state of a closed microcavity polariton system appears to be well described by its ground state.[14,16] In this study, assuming such a situation, we determine the ground state for a fixed excitation density at zero temperature as a function of experimentally variable parameters, i.e., excitation density and detuning,[19] and ultraviolet cutoff determined by the lattice constant.[18,20,21] In past studies, mean-field theories have been used to discuss the low excitation density[22,23] and high excitation density[24,25] by considering two different models. These theories are complementary,[26] but their relationship is somewhat ambiguous. Here, we also investigate the medium-density region where the electron-hole (e-h) wave function of the relative motion assumes importance. It is shown that the ground-state energy and wave function change gradually from those of excitons to photons as the excitation density increases. The change can be a crossover or a first-order transition, depending on the parameters considered. The latter is characterized by a jump in the photonic fraction, and a sudden narrowing of the e-h wave function that is accompanied by a change in the binding force from Coulombic force to photon-mediated force. The momentum distribution function and the excitation spectrum are also evaluated with the change in the ground states.

This paper is organized as follows. In Sec. II, we explain a model Hamiltonian describing the polariton systems in semiconductor microcavities. In Sec. III, we describe the variational approach employed to determine the ground state. We also introduce the interpolating wave functions for the polariton systems. In Secs. IV and V, the results obtained for a small cutoff and a large cutoff are shown, respectively. These results are compared to ascertain whether the evolution of the system ground state is a smooth crossover or involves

a first-order transition. In Secs. IV F and IV G, we carefully compare our results obtained using an interpolation method with those obtained using other models for the low-density and high-density limits.[22,23,25] We summarize our conclusions in Sec. VI.

II. MODELS

The polariton system can be regarded as consisting of electrons and photons with a total excitation number $N_{\rm ex}$, and interacting through electric-dipole coupling. The Hamiltonian is given by $H = H_{\rm el} + H_{\rm el\text{-}el} + H_{\rm ph} + H_{\rm el\text{-}ph}$,[25]

$$H_{\rm el} = \sum_k \xi_{e,k} e_k^\dagger e_k + \xi_{h,k} h_k^\dagger h_k, \tag{1}$$

$$H_{\rm el\text{-}el} = \sum_{q\neq 0} U_q \rho_q \rho_{-q}, \tag{2}$$

$$H_{\rm ph} = \sum_k [\sqrt{(ck)^2 + (\hbar\omega_c)^2} - \mu]\psi_k^\dagger \psi_k, \tag{3}$$

$$H_{\rm el\text{-}ph} = -g \sum_{k,q} (\psi_q e_{k+q}^\dagger h_{-k}^\dagger + \psi_q^\dagger h_{-k} e_{k+q}), \tag{4}$$

where $\xi_{e(h),k}[= \hbar^2 k^2/2m_{e(h)} + (E_g - \mu)/2]$ and $U_q[= \pi e^2/\epsilon^* Sq (= 2\pi e^2/\epsilon^* V q^2)]$ are momentum representations of the electronic dispersion in an effective-mass approximation and the Coulomb interaction potential for 2D (3D) systems, respectively. Here, the dielectric constant of a semiconductor material and the quantization area for 2D (3D) systems are given by ϵ^* and S (V), respectively. The reduced mass of an e-h pair is denoted by m_r. Further, e_k, h_k, and ψ_k are the annihilation operators of conduction electrons, valence holes, and photons with momentum k, respectively. The chemical potential μ is introduced to fix the number of total excitations $N_{\rm ex} \equiv \sum_k \psi_k^\dagger \psi_k + (e_k^\dagger e_k + h_k^\dagger h_k)/2$, which is conserved for the Hamiltonian. Accordingly, the term $-\mu N_{\rm ex}$ is included in the Hamiltonian. The Fourier transform of the density operator is given by $\rho_{q\neq 0} = \sum_k (e_{k+q}^\dagger e_k + h_{k+q}^\dagger h_k)$. The zero-point cavity frequency is denoted by ω_c, and the detuning parameter is defined as $d = (\hbar\omega_c - E_g)/\varepsilon_0$, where ε_0 is the exciton Rydberg energy in 3D systems. The light-matter coupling constant is given by $g = d_{cv}\sqrt{2\pi\hbar\omega_c/\epsilon^* S L_{\rm cav}} (= d_{cv}\sqrt{2\pi\hbar\omega_c/\epsilon^* V})$ for 2D (3D) systems. ($L_{\rm cav}$ is the effective cavity length.[27]) The momentum dependence of the dipole matrix element d_{cv} is neglected here. Instead, a momentum cutoff k_c is introduced so as to restrict the electronic states contributing to the polariton formation to $|k| < k_c$. It is smaller than or roughly equal to the inverse of the lattice spacing (e.g., $60/a_0$ for a GaAs-based microcavity, with a_0 being the exciton Bohr radius).

III. VARIATIONAL APPROACH FOR TWO- AND THREE-DIMENSIONAL SYSTEMS

Considering the coherent state of polarizations and photons, the mean-field ground state of a polariton condensate is given by

$$|\Phi\rangle = e^{(\lambda\psi_0^\dagger - \lambda\psi_0)} \prod_k (e^{i\chi_k} u_k + v_k e_k^\dagger h_{-k}^\dagger)|{\rm vac}\rangle, \tag{5}$$

where $|{\rm vac}\rangle$ denotes the vacuum state with no conduction electrons, no valence holes, and no excited photons. The normalization condition, $u_k^2 + v_k^2 = 1$, allows us to include the phase-space filling effects of fermions. Without the loss of generality, we can parametrize $u_k = \cos\theta_k$ and $v_k = \sin\theta_k$. The variational parameters λ, χ_k, u_k, and v_k are determined by minimizing the total energy $E(= \langle H + \mu N_{\rm ex}\rangle)$ for a fixed $\langle N_{\rm ex}\rangle$. In the coherent state, all the e-h pairs are found to have the same phase: $\chi_k = 0$.[22]

After angular integration, for 2D systems, the mean-field energy per excitation $\varepsilon(= E/N_{\rm ex})$ and the total excitation density $\rho_{\rm ex}(= N_{\rm ex}/S)$ are given by

$$\varepsilon/\varepsilon_0 = \frac{R_s^2}{a_0^2}\left(d\tilde{\lambda}^2 + \frac{1}{2}\int_0^{\kappa_c} \kappa^3 v_k^2 {\rm d}\kappa - \tilde{g}\tilde{\lambda}\int_0^{\kappa_c} \kappa u_k v_k {\rm d}\kappa - \int_0^{\kappa_c}\int_0^{\kappa_c} Q^{\rm 2D}_{\kappa_1,\kappa_2}(v_{k1}^2 v_{k2}^2 + u_{k1}v_{k1}u_{k2}v_{k2}){\rm d}\kappa_1 {\rm d}\kappa_2\right), \tag{6}$$

$$\rho_{\rm ex} = \frac{1}{\pi a_0^2}\left(\tilde{\lambda}^2 + \frac{1}{2}\int_0^{\kappa_c} \kappa v_k^2 {\rm d}\kappa\right) \equiv \frac{1}{\pi R_s^2}, \tag{7}$$

where $\kappa = k a_0$, $\kappa_c = k_c a_0$, and $Q^{\rm 2D}_{\kappa_1,\kappa_2} = \frac{2\kappa_1\kappa_2}{\pi(\kappa_1+\kappa_2)} K_1(\frac{4\kappa_1\kappa_2}{(\kappa_1+\kappa_2)^2})$, with $K_1(z)$ being the complete elliptic integral of the first kind, R_s being the mean separation, $\tilde{\lambda}(= \lambda\sqrt{\pi a_0^2/S})$ being the normalized photon field amplitude, and $\tilde{g}(= g\sqrt{S/\pi a_0^2 \varepsilon_0^2})$ being a dimensionless coupling constant. For 3D systems, $\varepsilon(= E/N_{\rm ex})$ and $\rho_{\rm ex}(= N_{\rm ex}/V)$ are similarly given by

$$\varepsilon/\varepsilon_0 = \frac{R_s^3}{a_0^3}\left(d\tilde{\lambda}^2 + \frac{2}{3\pi}\int_0^{\kappa_c} \kappa^4 v_k^2 {\rm d}\kappa - \tilde{g}\tilde{\lambda}\int_0^{\kappa_c} \kappa^2 u_k v_k {\rm d}\kappa - \int_0^{\kappa_c}\int_0^{\kappa_c} Q^{\rm 3D}_{\kappa_1,\kappa_2}(v_{k1}^2 v_{k2}^2 + u_{k1}v_{k1}u_{k2}v_{k2}){\rm d}\kappa_1 {\rm d}\kappa_2\right), \tag{8}$$

$$\rho_{\rm ex} = \frac{3}{4\pi a_0^3}\left(\tilde{\lambda}^2 + \frac{2}{3\pi}\int_0^{\kappa_c} \kappa^2 v_k^2 {\rm d}\kappa\right) = \frac{3}{4\pi R_s^3}, \tag{9}$$

where $\kappa = k a_0$, $\kappa_c = k_c a_0$, $Q^{\rm 3D}_{\kappa_1,\kappa_2} = \frac{4\kappa_1\kappa_2}{3\pi^2}\ln|\frac{\kappa_1+\kappa_2}{\kappa_1-\kappa_2}|$, R_s is the mean separation, $\tilde{\lambda}$ is the normalized photon field amplitude given by $\tilde{\lambda} = \lambda\sqrt{4\pi a_0^3/3V}$, and $\tilde{g}(= g\sqrt{3V/4\pi a_0^3\varepsilon_0^2})$ is a dimensionless coupling constant.

It is convenient to use an approximate interpolation method for the excitonic constituent,[28] rather than treat an infinite numbers of variational parameters u_k and v_k for all k. For 2D systems, we use the following formulas:

$$\frac{u_k v_k}{u_k^2 - v_k^2} = \frac{\zeta\ {\rm sgn}[(\kappa/2)^2 - \Omega]}{\sqrt{1 + (\kappa/2)^2}\sqrt{(\kappa/2)^4 - 2\Omega(\kappa/2)^2 + \eta^2\Omega^2}}. \tag{10}$$

This form of the wave function is chosen so as to guarantee correct results for three limiting cases: (i) exciton BEC [$\tilde{\lambda}R_s \ll a_0$, $\zeta \ll 1$, $\Omega = -1$, $\eta = 1$]—the low-density limit with a negligible photonic fraction, (ii) electron-hole plasma [$\tilde{\lambda}R_s \ll a_0$, $\zeta \ll 1$, $\Omega = (k_F a_0/2)^2$, $\eta = 1$]—the high-density limit with a negligible photonic fraction, and (iii) photonic BEC [$\tilde{\lambda}R_s \to a_0$, $\eta = 0$, $\zeta/\sqrt{|\Omega|}$ is finite while $\zeta = \infty$, $\Omega = -\infty$]—the photon-dominated regime with a small excitonic

fraction. For 3D systems, we directly use a wave function proposed by Comte and Nozieres,[28]

$$\frac{u_k v_k}{u_k^2 - v_k^2} = \frac{\zeta}{(1+\kappa^2)(\kappa^2 - \Omega)}. \tag{11}$$

This functional form also covers the above-mentioned three limits: (i) $\tilde{\lambda}^{2/3} R_s \ll a_0$, $\zeta \ll 1$, $\Omega = -1$; (ii) $\tilde{\lambda}^{2/3} R_s \ll a_0$, $\zeta \ll 1$, $\Omega = (k_F a_0)^2$; and (iii) $\tilde{\lambda}^{2/3} R_s \to a_0$, $\zeta/|\Omega|$ is finite while $\zeta = \infty$, $\Omega = -\infty$.

Limits (i) and (ii) are already known for the problem of BEC-BCS crossover in electron-hole systems.[28] As for the limit unique to the polariton systems, i.e., (iii), the parameter is defined to ensure $v_k \propto 1/k^2 (\ll 1)$ at a large momentum, which will be shown in Sec. V. With the interpolating wave functions defined above, we can discuss the crossover of the ground states among the three limits via polariton BEC. We solve the variational problem in terms of the four parameters ζ, Ω, η, and λ for 2D systems, and the three parameters ζ, Ω, and λ for 3D systems.

IV. RESULTS FOR A SMALL CUTOFF

In this section, we will present the solution to the variational problem when the cutoff parameter k_c is chosen not too large. In this case, the cutoff effect is weak and the variational ground states change smoothly for all excitation densities and for all values of d. The case of a very large cutoff parameter is discussed in Sec. V.

A. Energy per particle and chemical potential

Figure 1 shows the mean-field energy per excitation (ε) and the chemical potential (μ) plotted as a function of R_s with a varying detuning parameter. Here, μ is evaluated using a variational equation $\partial\langle H\rangle/\partial\lambda = 0$ that reduces to

$$\mu = \hbar\omega_c - \frac{g}{2\lambda}\sum_k u_k v_k. \tag{12}$$

Both ε and μ are monotonic in R_s for both 2D and 3D systems.

In the weak-coupling case with large detuning, $\hbar\omega_c -$ (exciton level) $\gg \tilde{g}$, ε and μ are positioned at the energy levels of a single exciton in the low-density limit with large R_s: $\varepsilon/\varepsilon_0$, $\mu/\varepsilon_0 \to -4$ for 2D and $\varepsilon/\varepsilon_0$, $\mu/\varepsilon_0 \to -1$ for 3D. On the other hand, for the strong-coupling case, $\hbar\omega_c -$ (exciton level) $\leqslant O(\tilde{g})$, ε and μ separate from the single exciton level for large R_s, because the carriers are already coupled with the photons in the low-density limit. Thus, ε and μ are rather given by the energy levels of a single polariton in the strong-coupling case: $d = -3, 0$ in Figs. 1(a) and 1(b), and $d = -0.7$ in Figs. 1(c) and 1(d). As the density increases (R_s decreases), ε and μ increase monotonically and follow the dashed curves obtained for electron-hole systems without a cavity in Ref. 28 (Comte-Nozieres) for large d. On the other hand, they gradually deviate from the dashed curves for small d. In the high-density limit $R_s \ll a_0$, ε and μ saturate at energy levels below the photon levels for any value of d.

The energy saturation at high density is explained by fermionic phase-space filling. The number of e-h pairs increases until the conduction electron band is filled up to the photon level, and thereafter, photonic excitations replace those

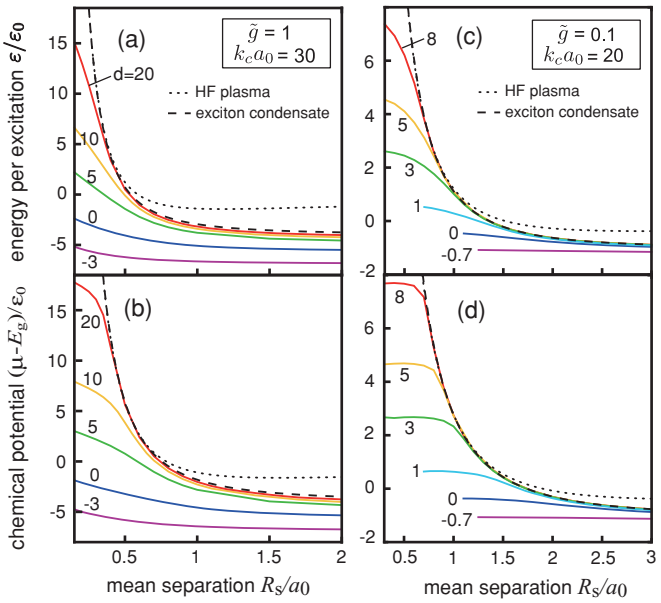

FIG. 1. (Color online) Energy per excitation ε plotted as a function of R_s for (a) 2D systems with $\tilde{g} = 1$ and $k_c a_0 = 30$ and (c) 3D systems with $\tilde{g} = 0.1$ and $k_c a_0 = 20$, for various d. The chemical potential μ is plotted as a function of R_s for (b) 2D systems and (d) 3D systems, respectively, for the same sets of d as (a) and (c). The dashed curves are obtained by applying the theory of exciton condensation.[28] The dotted curves denote the results for electron-hole (e-h) plasma.

of e-h pairs to minimize the total energy (Fig. 2). This simple explanation can be applied to the case of weak coupling with large d and small $\tilde{g}$; however, it cannot be applied to the case of strong coupling with small d and large $\tilde{g}$ because both photons and carriers exist even in the low-density limit (although it is correct qualitatively). The photonic characteristic is observed above the density ($R_s < R_s^*$), where ε and μ deviate from the dashed curves.

The overall results can be roughly summarized as follows: the excitation energy in the ground states of polariton condensates changes from that of a single exciton to cavity photons, indicating that the ground states change from excitonic to photonic with an increase in the density.

B. Photon and carrier density

The crossover from excitonic BEC to photonic BEC referred to in the previous subsection can be verified directly from the R_s dependency of the photonic fraction in the polariton condensates ($\tilde{\lambda}^2 R_s^2$ in 2D systems, and $\tilde{\lambda}^2 R_s^3$ in 3D systems), which is shown in Fig. 3 [(a) for 2D systems and (b) for 3D systems]. The photonic fraction is also monotonic in R_s. For the weak-coupling case with large d, it increases sharply from zero at the onset of R_s, which corresponds to R_s^* mentioned above. Above the onset density ($R_s < R_s^*$), the polariton condensates exhibit photonic characteristics. For the strong-coupling case with small d, the photonic fraction is already finite in the low-density limit; hence, there is no onset density above which the photonic characteristic appears. This is consistent with the observation in Fig. 1 that the energies ε and μ largely deviate from that of the exciton BEC in the

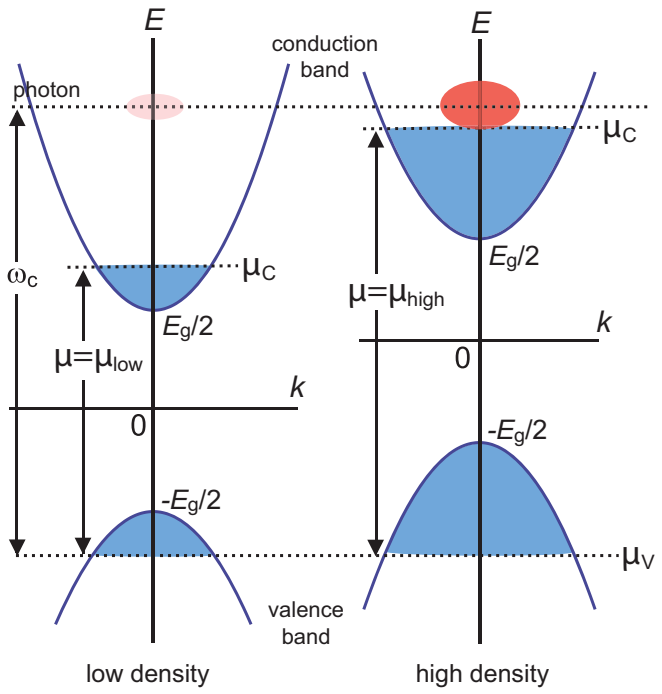

FIG. 2. (Color online) Energy saturation found in Fig. 1. ($\mu \equiv \mu_C - \mu_V$ in the figure.)

low-density limit for small d. These characteristics are similar for both 2D and 3D systems.

In Fig. 4, we plot the densities of photons ($n_{\rm ph}$) and carriers ($n_{\rm car}$) as a function of the total excitation density ($n_{\rm tot}$) for various d. For the strong-coupling case, densities of both photons and carriers increase together with $n_{\rm tot}$ from the low-density limit, and the clear onset is not observed. On the other hand, for the weak-coupling case with large d, the sharp onset (inverted triangles in Fig. 4) like the input-output curves of lasers is found clearly as well as in Refs. 29, 25, and 21. At the onset, the increase of $n_{\rm ph}$ and the saturation of $n_{\rm car}$ start sharply. The crossover between the smooth and sharp onsets can be understood physically as follows. The laserlike behavior with a sharp onset is observed if d is large and if the values of ε and μ at the onset R_s^* are close to those of e-h plasma (dotted line in Fig. 1). In this case, the carriers are considered to form e-h plasma, and electrons and holes are

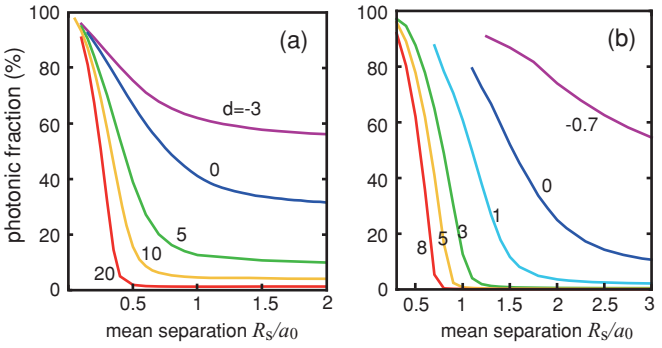

FIG. 3. (Color online) Photonic fraction plotted as function of R_s for (a) 2D systems and (b) 3D systems, for various d. The same parameter sets are used as those in Figs. 1(a) and 1(b), respectively.

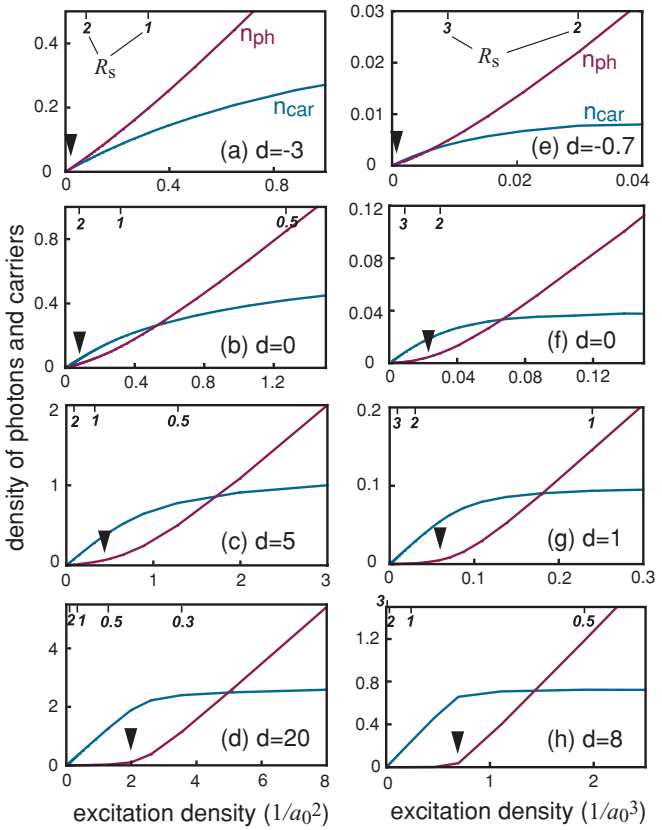

FIG. 4. (Color online) Photon and carrier density in polariton condensates as a function of total excitation density $n_{\rm tot}$: for 2D systems with (a) $d = -3$, (b) $d = 0$, (c) $d = 5$, and (d) $d = 20$ and for 3D systems with (e) $d = -0.7$, (f) $d = 0$, (g) $d = 1$, and (h) $d = 8$. Other parameters are the same as those in Fig. 1. In the upper horizontal axes of each figure, the corresponding R_s values are indicated. The onset densities where $n_{\rm ph}$ starts to increase are marked by inverted triangles. For large d, curves are similar to input vs output and input vs inversion-population curves typical of lasers.

unbound for $R_s < R_s^*$. This situation is quite similar to the case of conventional semiconductor lasers at high carrier density with negligible Coulomb interaction. On the other hand, for the case of strong coupling with small d, the particles that tend to form condensates are the polaritons—a mixed state of an exciton and a photon—at low density. Thus, $n_{\rm ph}$ increases with excitation at low density; hence, it shows the smooth onset of the photon density.

C. Microscopic properties: Momentum distribution of carriers and the wave function of e-h pairs

In the preceding subsections, we discussed macroscopic quantities such as ground-state energies and photon and carrier densities. Here, we focus on microscopic properties.

Figure 5 shows the momentum distribution of carriers [$f_e(k) = f_h(k)$] given by $\langle e_k^\dagger e_k \rangle = v_k^2$ at various R_s and d for 2D [Figs. 5(a)–5(c)] and 3D [Figs. 5(d) and 5(e)] systems. For the strong-coupling case with small d, $f_e(k)$ does not exceed 0.5 for all k and over the entire density regime, i.e., there is no inversion population [e.g., see Figs. 5(a) and 5(b)]. For the weak-coupling case with large d, on the other hand, $f_e(k)$

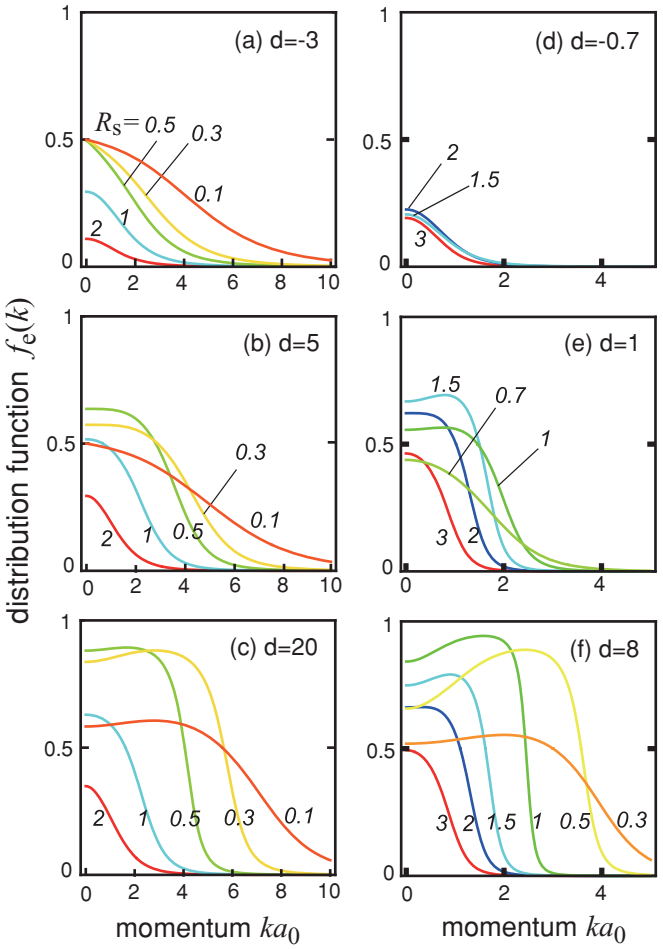

FIG. 5. (Color online) Momentum distribution of carriers $\langle a_k^\dagger a_k\rangle = v_k^2$ for various R_s and d: for 2D systems with (a) $d = -3$, (b) $d = 5$, and (c) $d = 20$ and for 3D systems with (d) $d = -0.7$, (e) $d = 1$, and (f) $d = 8$. Other parameters are the same as those in Fig. 1.

exceeds 0.5 and forms a Fermi surface at high density [e.g., see Fig. 5(c), $R_s = 0.5,0.3$]. This is because photonic excitation replaces carrier excitation at high density. For small d, the crossover density (corresponding to $R_s = R_s^*$) is small and the carrier density cannot be large. For large d, on the other hand, the carrier density can be sufficiently large to form a Fermi surface, because the crossover density is sufficiently high.

As the density increases (R_s decreases), the momentum distribution widens. In particular, for large d, the Fermi surface disappears at high density and a plateau is found at $f_e(k) \sim 0.5$ for small k [e.g., see Figs. 5(c), $R_s = 0.3 \to 0.1$, and 5(f), $R_s = 0.5 \to 0.3$]. This is due to minimization of total energy in the presence of the large coherent photons. As Eastham noted,[22] the polarization $\langle e_k^\dagger h_{-k}^\dagger\rangle = u_k v_k = \sin\theta_k \cos\theta_k$ tends to maximize up to 0.5 [which means $f_e(k) \to 0.5$] to minimize $\langle H_{\text{el-ph}}\rangle$ when the coherent photon field grows. At the same time, $f_e(k) \to 0$ for large k to minimize the kinetic energy. To minimize the sum of kinetic energy and $\langle H_{\text{el-ph}}\rangle$ in the photon-dominated regime, the broadening of $f_e(k)$ and the plateau at $f_e(k) \sim 0.5$ occur (Fig. 5). As shown in the latter section (Sec. V C), in the photon-dominated regime, the tails of $f_e(k)$ at large k change from k^{-6} to k^{-4} in 2D systems, and from k^{-8} to k^{-4} in 3D systems. The broadening of the large-k tail is also a result of the light-matter coupling.

An interesting point is the nonmonotonic dependence of the distribution function on the excitation density for large d and small k; $f_e(k)$ increases and the carrier population is inverted [$f_e(k) > 0.5$] in the medium density region until the photonic fraction is negligible. Above the onset density (inverted triangles in Fig. 4) where the photonic fraction becomes significant, the inverted population is depleted and $f_e(k)$ decreases to ~ 0.5. This feature is very similar to the *spectral hole burning* in a laser.[17] Besides, such nonmonotonic dependencies of $f_e(k)$ are found only when the relationship between the photon density and the excitation density exhibits a curve similar to the input-output curves of the laser shown in Fig. 4. Of course, there are differences between the depletions of the carrier populations in the photonic regime of the polariton condensates and in lasers. For lasers, the spectral hole in the carrier distribution is found only in the small spectral region, i.e., the width of the spectral hole in the momentum space is small and corresponds roughly to the natural linewidth of atomic transitions, γ_a. However, the depletion in the carrier distribution function spreads over the entire momentum space for the polariton condensates. Another difference is that the saturated value of the population is determined by nonequilibrium parameters such as cavity photon loss γ_{ph} and the natural linewidth of atoms γ_a in the case of the laser. In fact, the saturated inversion is roughly $\propto \gamma_a\gamma_{\text{ph}}/g^2$ in the case of lasers. On the other hand, the saturated inversion is ~ 0 [i.e., $f_e(k) \sim 0.5$] in the case of the polariton condensates. However, we neglected all the nonequilibrium loss parameters in our model. Therefore, we find that the results for a polariton BEC are consistent with those for lasers by setting $\gamma_a = \gamma_{\text{ph}} = 0$.

The light-matter coupling effect is also seen in the wave function of e-h pairs, $p_k = \langle a_k^\dagger b_k\rangle = u_k v_k$, as shown in Fig. 6. For small d, p_k increases with the density, and the broadening is already seen above relatively low density. For large d, p_k increases with the density at first. Thereafter, in the medium-density regime, p_k decreases for small k and increases for $k \sim k_F$ with a sharp peak, while the shape of the large k tail does not change. This indicates the formation of the Fermi surface. The carriers inside the Fermi sea cannot move freely; hence, they do not contribute to the polarization. In contrast, the carriers near the Fermi surface affect the polarization. In addition, for the medium-density regime, coherent photons do not affect the polarization. At the highest density with large d, the coherent photons play a major role; the dip at small k does not occur and a plateau is formed at the maximum value $p_k \sim 0.5$ while a long tail is found at large k. In the photon-dominated regime, the tails of p_k change from k^{-3} to k^{-2} in 2D systems, and from k^{-4} to k^{-2} in 3D systems.

D. Microscopic properties: Excitation spectrum of Bogoliubov quasiparticles

In this subsection, we discuss the energy spectrum measured to add (subtract) one e-h pair to (from) the ground state within the mean-field approximation. The energy spectrum is described by the mean-field theory similar to that of the excitation spectrum of Bogoliubov quasiparticles in BCS superconductors.[30] The energy spectrum will be observed in

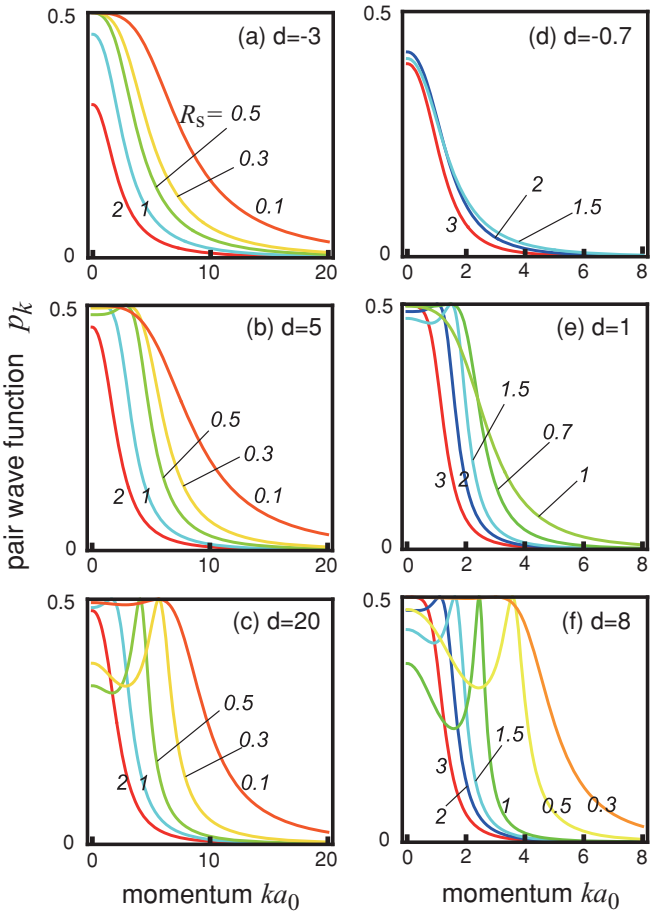

FIG. 6. (Color online) Momentum space profile of electron-hole pairs $p_k = \langle a_k^\dagger b_k \rangle$ for various R_s and d: for 2D systems with (a) $d = -3$, (b) $d = 5$, and (c) $d = 20$ and for 3D systems with (d) $d = -0.7$, (e) $d = 1$, and (f) $d = 8$. Other parameters are the same as those in Fig. 1.

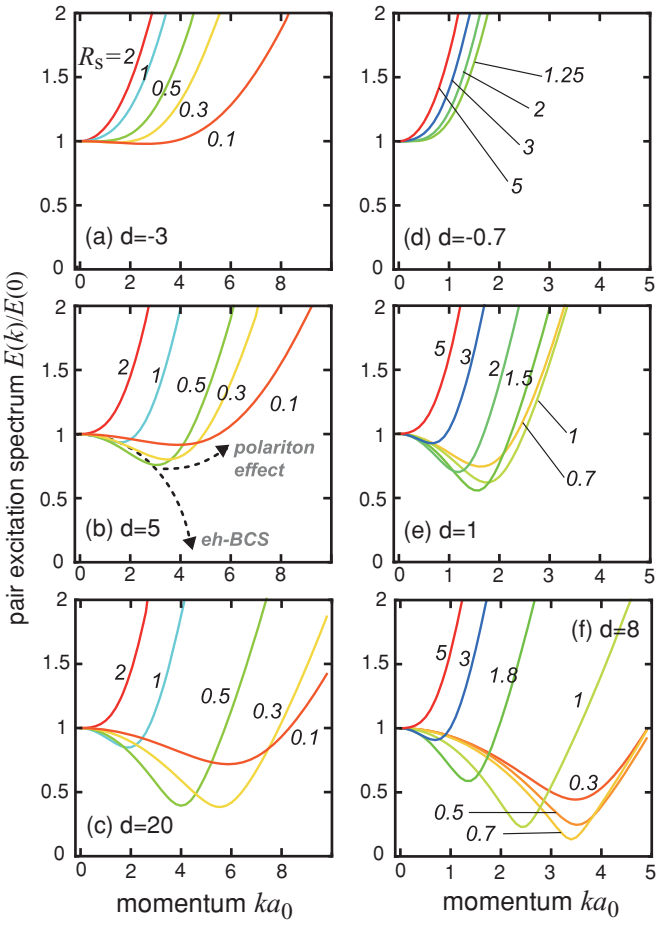

FIG. 7. (Color online) Excitation spectrum of carriers $E(k)/E(0)$ for various R_s and d: for 2D systems with (a) $d = -3$, (b) $d = 5$, and (c) $d = 20$ and for 3D systems with (d) $d = -0.7$, (e) $d = 1$, and (f) $d = 8$. Other parameters are the same as those in Fig. 1.

the emission and absorption spectrum.[23,31] The mean-field Hamiltonian for the carrier part is expressed as $H^{\rm mf} = \sum_k \Phi_k^\dagger \mathcal{H}_k^{\rm mf} \Phi_k$ in terms of $\Phi_k = (e_k, h_{-k}^\dagger)$ by neglecting the constant shift. The self-energy Σ_k and the pair gap Δ_k are given by

$$\mathcal{H}_k^{\rm mf} = \begin{pmatrix} \xi_{e,k} + \Sigma_k & \Delta_k \\ \Delta_k & -\xi_{h,k} - \Sigma_k \end{pmatrix},$$
$$\Sigma_k = -2\sum_{k'} U_{k-k'} v_{k'}^2, \qquad (13)$$
$$\Delta_k = -2\sum_{k'} U_{k-k'} u_{k'} v_{k'} - g\lambda.$$

After the Bogoliubov transformation, we determine the energy spectrum for the creation of an e-h pair as follows:

$$E_k^\pm = \frac{\xi_{e,k} - \xi_{h,k}}{2} \pm \sqrt{\left(\frac{\xi_{e,k} + \xi_{h,k}}{2} + \Sigma_k\right)^2 + \Delta_k^2}. \quad (14)$$

In the polariton ground state, the Fermi sea is filled with bogolons of the lower branch (E_k^-). Therefore, to create an e-h pair with momentum k in the ground state, energy $E(k) = E_k^+ - E_k^-$ is needed. We plot in Figs. 7 and 8 the pair-excitation spectrum $E(k)/E(0)$ and the density of states (DOS),

$$D(\omega - \mu) = \frac{1}{S}\sum_{k,\tau=\pm} \delta(\omega - \mu - E_k^\tau), \qquad (15)$$

for various d and R_s.

For small d [Figs. 7(a) and 7(d)], the excitation spectrum broadens as the density increases, and the value of k at the minimum energy stays almost constant at $k \sim 0$. In the high-density photonic region, the bottom of the energy band becomes flat, because the constant pair gap $-g\lambda$ plays a dominant role. Accordingly, the peak of the DOS becomes sharp and high in the photonic regime [$R_S < 0.5$ in Fig. 8(a)] whose position shifts to higher energies with $|g\lambda|$. This implies that, in the photon-dominated regime, e-h pairs are bound mainly by photon-mediated interaction while the Coulomb attraction has a small effect. The broadening of the spectrum in the k space can be directly interpreted as the e-h pairs having a size much smaller than the Bohr radius in real space. These effects originate from the fact that an e-h pair is created at the same position where photons are absorbed. This feature is discussed again in Sec. V.

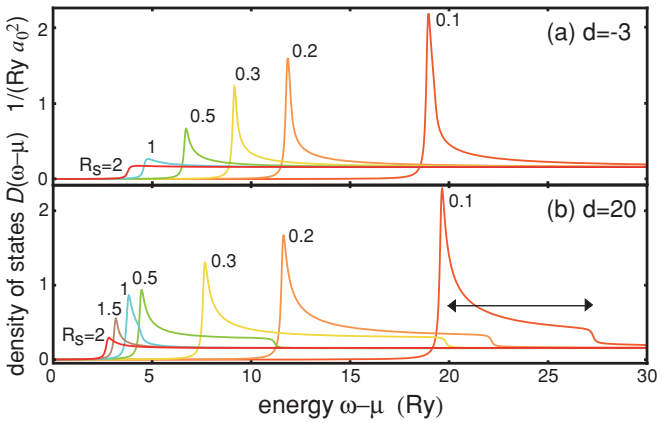

FIG. 8. (Color online) Density of states in Eq. (15) for 2D systems: (a) $d = -3$, (b) $d = 20$. A Lorentzian function with a width 0.1 Ry is used for the plot instead of using a Dirac δ function. Only the upper branch E_k^+ contributes for $\omega - \mu > 0$.

For large d [Figs. 7(c) and 7(f)], as the density increases, the value of k at the energy minimum changes from zero to $k > 0$ and the minimum of $E(k)/E(0)$ decreases. This reflects the formation of the Fermi surface, and the system enters from an e-h BEC regime into an e-h BCS regime. As the density increases, $\min[E(k)/E(0)] \sim \Delta_{k_F}/\varepsilon_F$ decreases, and becomes zero if the system enters an e-h plasma regime [the lower dashed arrow in Fig. 7(b)]. In the e-h BCS regime, in addition to the peak, a steplike change is found in the DOS [$R_S < 1$ in Fig. 8(b)]. The steplike change is due to the nonmonotonic shape of the spectrum in k space, which originates from the existence of the Fermi surface. This feature of an excitonlike regime is exactly the same as the result of Comte-Nozieres.[28] At high density ($R_s < R_s^*$), the coherent photon develops in the condensate, and the constant pair gap $-g\lambda$ becomes dominant. As a result, the bottom of the energy band becomes flat and broadening is seen in the k space. Accordingly, the peak in the DOS becomes sharp and high, and the width of the step region [length of the arrow in Fig. 8(b)] decreases with the density (for $R_S < 0.2$). For the higher density in the photonic regime, the step will disappear.

In Fig. 9, we plot the minimum energy needed for breaking an e-h pair, $E_{\min} = E(k = k_{\min})$, as a function of the mean separation between carriers $r_s = \sqrt{1/\pi n_{\rm car}}$ given by the carrier density $n_{\rm car}$, for various detunings (solid lines). The dashed lines show the results of exciton BEC without the cavity photons, where we can clearly see the BEC-BCS crossover of the e-h pair, i.e., the pair gap smoothly changes from the exciton binding energy at low density (large r_s) to small values decreasing with $n_{\rm car}$ at high density. For large detunings, the pair gap of the polariton systems is almost the same as that of the exciton condensates at low density, because the photonic fraction is almost zero. Once the photonic fraction become finite, the pair gap increases with the photonic components and eventually diverges at the high excitation density. This implies that electrons and holes are strongly bound because of an increase in the photon-mediated attraction. As seen at $d = 8$ in Fig. 9(b), for very large detunings, the pair gap can have a nonmonotonic dependency on the density. For small detunings, $E_{\min}$ shows a monotonic increase and becomes greater than the value for the exciton condensates.

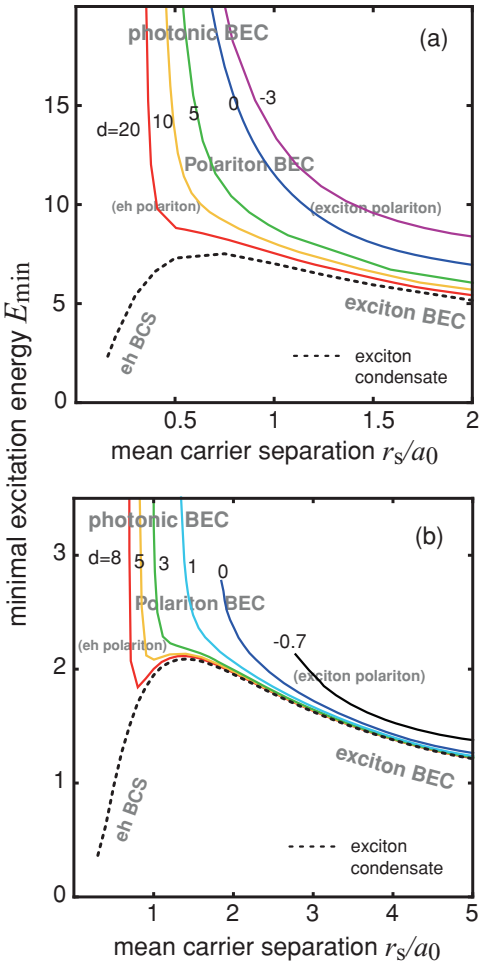

FIG. 9. (Color online) Minimal excitation energy $E_{\min}$ needed for breaking the e-h pair plotted as a function of mean separation between carriers: (a) 2D systems where $r_s = (\pi n_{\rm car})^{-1/2}$ and (b) 3D systems where $r_s = (4\pi n_{\rm car}/3)^{-1/3}$.

E. Phase diagram

Figure 10 shows zero-temperature phase diagrams for 2D and 3D systems, with small cutoff. They consist of four different phases, as explained below.

In the excitonic regime where $R_s > R_s^*$, the ground state is classified into two groups even though there are no clear boundaries. This is well known in the theory of the BEC-BCS crossover of electron-hole systems.[28] If the energy level of one-particle excitation in e-h systems (dashed curves in Fig. 1) is close to the single-exciton level $-4\varepsilon_0$, the e-h pairs can be regarded as exciton condensates. Thus, the low-density regime ($R_s \gtrsim 1$ for 2D systems and $R_s \gtrsim 2$ for 3D systems) is categorized as an "exciton BEC." For higher densities ($R_s \lesssim 1$ for 2D systems and $R_s \lesssim 2$ for 3D systems), which are categorized as "e-h BCS," e-h pairs are regarded as weakly bound fermions such as Cooper pairs in BCS superconductors. In the highest density regime of e-h BCS ($R_s \lesssim 0.4$ for 2D systems and $R_s \lesssim 1$ for 3D systems), the curve of the e-h system (dashed line in Fig. 1) overlaps with that of the e-h plasma (dotted line in Fig. 1). In this regime, e-h pairs are almost unbound like e-h plasma and all excitations are fermionic. Because R_s^* varies, d determines the regimes

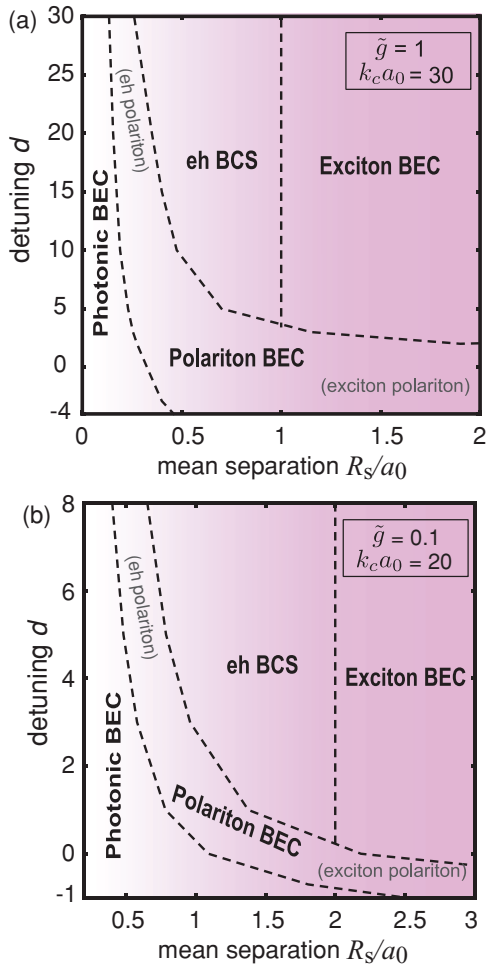

FIG. 10. (Color online) Phase diagram of a polariton system in (d, R_s) space for small cutoff: (a) 2D systems with $\tilde{g} = 1, k_c a_0 = 30$, (b) 3D systems with $\tilde{g} = 0.1$, $k_c a_0 = 20$. The changes between different phases are crossover, and the phase boundaries are shown by dashed lines. The region where Coulomb attraction dominates the photon-mediated interaction in the formation of e-h pairs is shaded (pink).

through which the polariton system passes—exciton BEC and e-h BCS—before the ground state becomes photonlike.

In addition to the two excitonic phases—exciton BEC and e-h BCS—the phase diagram contains a "polariton BEC" phase and a "photonic BEC" phase. Although we observe large coherent polarization and coherent photons in the latter two phases, we classify them as follows: excitations of carriers and cavity photons both make a major contribution to the formation of the condensates in the polariton BEC phase. On the other hand, photonic excitations dominate carrier excitation in the photonic BEC phase. All the ground states cross over in the phases stated above; hence, the boundaries between different phases are determined under certain conditions.[32] As seen in the phase diagram, the detuning parameter determines how the condensate evolves from the low-density to the high-density regime. For large detunings, the system experiences four types of ground states from (to) exciton BEC, e-h BCS, polariton BEC, and photonic BEC. For small detunings, the ground state changes from a polariton BEC to a photonic BEC.

The phase diagrams are quite similar for 2D and 3D systems in the case of small cutoff. The area of a polariton BEC phase is larger in Fig. 10(a) than in Fig. 10(b); however, the difference arises from our choice of coupling parameters g, and not from the dimensionality.

F. Comparison with other models in the low-density limit

In this subsection, we compare our results to those obtained with other models for the low-density limit.[22,23] Eastham[22] and Keeling[23] studied the ground states and the fluctuations around them in the low-density limits by using a generalized Dicke model.[33] In their works, they assumed an ensemble of two-level atoms that interact with photons and not directly with the other atoms by Coulomb force. Thus, the interaction between atoms is only possible through interaction with photons. The energy dispersion of the atomic transition is described by a Gaussian distribution with a finite width. An advantage of neglecting the two-body interaction is that the full incorporation of the single occupancy conditions for each atom, i.e., the Pauli blocking effect, is possible in the path-integral formalism.[22,23,34]

The results obtained in Ref. 22 for the electronic distribution (Fig. 2 of Ref. 22) can be compared with those shown in Fig. 5 in our paper. In Ref. 22, the distribution function changes with an increase in the density as follows: (i) The Fermi step shifts upward near the photon level and then broadens because coupling to photons results in coherent polarization. In other words, the e-h pair almost reaches the resonance level. (ii) In the high-density limit, the excitations become photonic and all atoms show Rabi oscillation by following the photonic field oscillation. (iii) As a result, the electronic occupancy is fixed at 0.5. The Fermi step observed at low density for their model is as expected because coupling with photons and polarization does not occur. However, our analysis reveals different results. Because of the intrinsic Coulomb interaction between electrons and holes, the polarization occurs before photonic excitation and there is no Fermi step at low density. This feature is usually observed in excitonic insulators.[28] Owing to the Coulomb interaction, the distribution function $f_e(k)$ in Fig. 5 appears similar to the wave function of a $1s$ exciton $f_e(k) \propto |\varphi_{1s}(k)|^2$ at low density. Further, similar to the analysis results of the Dicke model, our results also show a broadening in the Fermi step in the medium-density regime and a plateau at 0.5 in the high-density regime.

G. Comparison with other model in the high-density limit

In this subsection, we compare our results with those obtained using two-band models of semiconductor carriers in the high-density limit.[24,25] They are based on the high-density approximation in the weak-coupling limit (the pair potential $\Delta \ll \varepsilon_F$ in their papers), which assumes the well-defined Fermi surface. Further, Marchetti[25] assumed the screened Coulomb potential, which is reasonably treated by a short-range contact potential with the strength $V \propto (1 + 8n_{\rm car}a_0^2/\pi)^{-1/2}$. Due to the screening effect, the pair gap decreases with the density in the excitonic regime. Contrary to that, at large density where photon-mediated attraction becomes dominant, the pair gap increases with the density.

This results in the nonmonotonic change in the pair gap as a function of the density (Fig. 6 of Marchetti[25]). Marchetti's model for the photon-dominated regime can be replaced by the free-carrier theory by Aleksandrov,[24] where the pair gap is given by $g\lambda$.

Our model reproduces the result of weak-coupling theories including the nonmonotonic dependence (Fig. 9) for large detunings between the e-h BCS phase and the (e-h) polariton BEC phase. (See also Fig. 1 of Ref. 24 for the comparison with the DOS in Fig. 8.) In our model, however, the Fermi surface is completely smoothed and the distribution function becomes flat at $f_e(k) \sim 0.5$ for the larger density in the photonic regime. There, as they noticed,[25] the weak-coupling theory fails since the assumption ($\Delta \ll \varepsilon_F$) does not hold. Therefore, our model extends the past theories not only to the low densities, but also to the high-density limit of photonic condensates $g\lambda \gg \mu - E_g$.

Another difference from Marchetti[25] is that our model uses the bare Coulomb potential with no screening effects. However, being similar to them, the pair gap decreases with the density, as shown in Fig. 9 in the e-h-BCS regime, because the formation of e-h pairs is possible only around the Fermi surface [peaks at the Fermi surface in Figs. 7(c) and 7(f)]. For high carrier density in 2D systems, the restriction of the phase space of scattering processes reduces the Coulomb interaction to a greater extent than screening does. In fact, the strength of the bare Coulomb attraction for the e-h pair decreases with the density roughly as $1/k_F \propto (n_{\rm car})^{-1/2}$ for 2D systems. In the high-density regime, the dependency is approximately the same for the screened model, $\propto (1 + 8n_{\rm car}a_0^2/\pi)^{-1/2}$. Thus, our model gives results similar to those of the screened model for the e-h-BCS regime. An advantage of our interpolation method is that we do not need to assume that a Fermi surface exists. As noted in Sec. III, our theory can interpolate among three limits of (i) exciton BEC, (ii) e-h plasma, and (iii) photonic BEC.

V. RESULTS FOR A LARGE CUTOFF

In this section, we will present the solution to the variational problem when the cutoff parameter k_c is large. In this case, there arises a possibility for the first-order transition to occur at high density owing to the large cutoff, especially for 3D systems. This is because the dipole-coupling parameter does not depend on the momentum of carrier excitation [see Eq. (4)]; in other words, each photon forms a pair of an electron and hole at the same position. A photon-mediated binding force introduces an attractive δ potential for the e-h pairs, and the divergence of the binding energy without any short-distance cutoff. The smallest length scale is the lattice constant of semiconductors, and it affects the ground states of polariton condensates. Here, we focus on such short-distance effects in more detail.

A. Short-distance cutoff: Possibility of first-order transition

For a small cutoff, the variational problem always has one solution that can smoothly connect the three limits of different types of ground states, (i)–(iii) referred to in Sec. III,

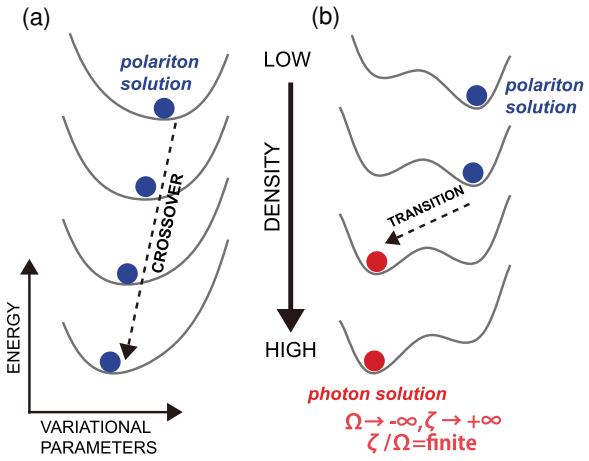

FIG. 11. (Color online) Change in the solution to the variational problem. While an energy minimum (polariton solution) gradually changes for small cutoff k_c (a), the system ground state switches to another minimum (photon solution) for large cutoff k_c (b).

at different densities. We will call this solution a "*polariton solution*." For a polariton solution, the polariton BEC gradually approaches the limit of (iii) a photonic BEC [Fig. 11(a)]. For a large cutoff, the energy profile within the space of variational parameters shows an additional minimum even at low excitation density. The corresponding solution is different from the polariton solution and is located near the limit of (iii) in the parameter space. We will call this solution a "*photon solution*." As shown in Fig. 11(b), the total energy of the polariton solution is less than that of the photon solution at low density. However, at a certain density, the energy of the photon solution becomes less than that of the polariton solution. This clearly suggests the possibility of the occurrence of a first-order transition from the polariton solution to the photon solution.

In Figs. 12(a) and 12(b), we show the R_s dependencies of the ground-state energy per excitation and photonic fraction in

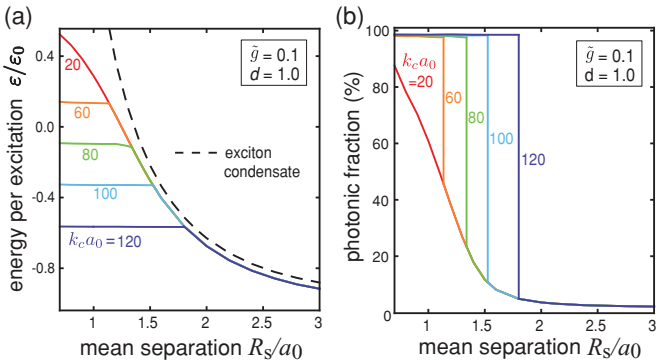

FIG. 12. (Color online) (a) Energy per excitation ε and (b) photonic fraction are plotted as a function of R_s for various cutoff parameters $k_c a_0 = 20$, 60, 80, 100, and 120 and for 3D systems with $d = 1$, $\tilde{g} = 0.1$. The dashed curve in (a) represents the result obtained by applying the theory of exciton condensation.[28]

the condensate, calculated for $d = 1$ and various values of k_c. The change in the polariton state at $k_c a_0 = 60$, 80, 100, and 120 is not a crossover but rather a first-order transition because of a discontinuous jump in the slope of the curve in Fig. 12(a). Similarly, as shown in Fig. 12(b), the photonic fraction jumps to almost 100% at the transition density. The system ground state is described by the photon solution in the high-density regime where the photonic fraction is almost 100%. The energy of the photon solution is almost independent of the density whose value decreases with an increase in k_c. This is due to the enhancement of the binding energy by the photon-mediated short-range attraction for large k_c. This point is discussed in Sec. V C in further detail. For large $k_c a_0$, the energy of the photon solution is always below that of the polariton solution for all densities. However, this situation arises only when the cutoff parameter is chosen to be unrealistically large.

The first-order transition observed with a jump in the chemical potential in Refs. 22 and 23 (e.g., Fig. 1 of Ref. 22) for large detunings should be mentioned here. The physics of the transition studied therein is different from the one found in our model. The former transition is explained by the symmetry of a Gaussian distribution of atomic transition energies about the center. For large detunings, the dipole interaction energy $H_{\text{el-ph}}$ increases from zero to the maximum value and then decreases to zero when the atomic excitation increases from zero to that for half-filling and then to that for full occupancy. Owing to the nonmonotonic change in the dipole coupling strength, the photonic density increases and decreases again from zero to that at full occupancy of atomic excitations. Above the density at full occupancy of atoms, the photonic excitation dominates and increases again. The nonmonotonic dependency of the photon amplitude (Fig. 3 of Ref. 22) causes a first-order transition from excitonic to photonic condensation.[23] Indeed, the transition occurs only for large detunings. The symmetry is not observed for small detunings because the photonic excitation increases monotonically with the excitation density. The transition is also affected by inhomogeneous broadening, especially of the bandwidth, because the symmetry is lost if the strength of the coupling to photons depends on the energy separation of atomic transition from the photon level. Thus, the jump in the chemical potential is smooth for a large bandwidth (see Fig. 1 of Ref. 22).

These features of the first-order transition observed for the generalized Dicke model are different from the ones found in our study, because we assume the effective bandwidth given by the cutoff parameter k_c is always large such that the cavity-mode frequency is within the continuum of the atomic transition. Thus, the occupation of the full bandwidth does not occur owing to the carrier saturation discussed in Secs. IV A and IV B. The first-order transition in our model occurs because of the large cutoff, i.e., large bandwidth, rather than the detuning; it occurs even at small detunings. In our study, the jump is found in the photon amplitude (Fig. 12) instead of the chemical potential observed by Eastham and Keeling. The transition found in our model, as shown later, is rather attributed to the formation of a strongly bound state of the e-h pairs due to the photon-mediated short-range attraction, which is sensitive to the cutoff of large momentum states of carriers.

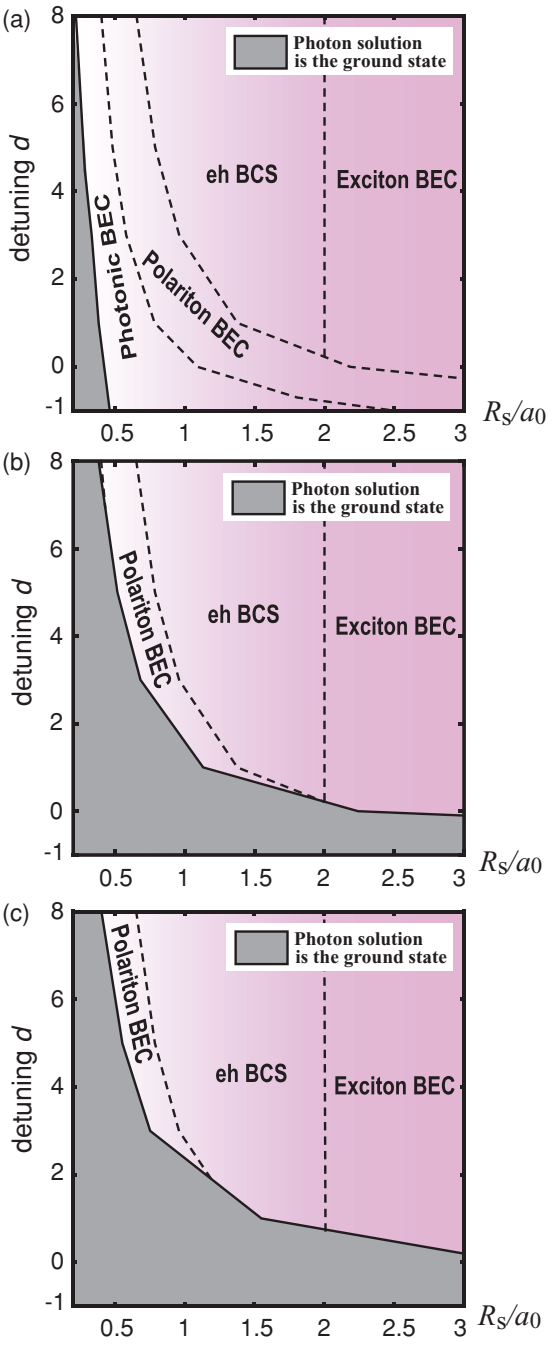

FIG. 13. (Color online) Phase diagram of 3D polariton system in (d, R_s) space (same as Fig. 10) for $\tilde{g} = 0.1$ and large cutoff parameters: (a) $k_c a_0 = 40$, (b) $k_c a_0 = 60$, and (c) $k_c a_0 = 100$. In the gray area, the photon solutions become the ground state. The first-order transition from the polariton solution to the photon solution occurs at the boundary. The dashed lines show that the changes between different phases correspond to a crossover. The region where Coulomb attraction dominates the photon-mediated interaction in the formation of e-h pairs is colored (pink).

B. Phase diagram

Figure 13 shows phase diagrams in the (d, R_s) space for large cutoff parameters. The polariton solution is almost independent of the cutoff parameter. Therefore, the

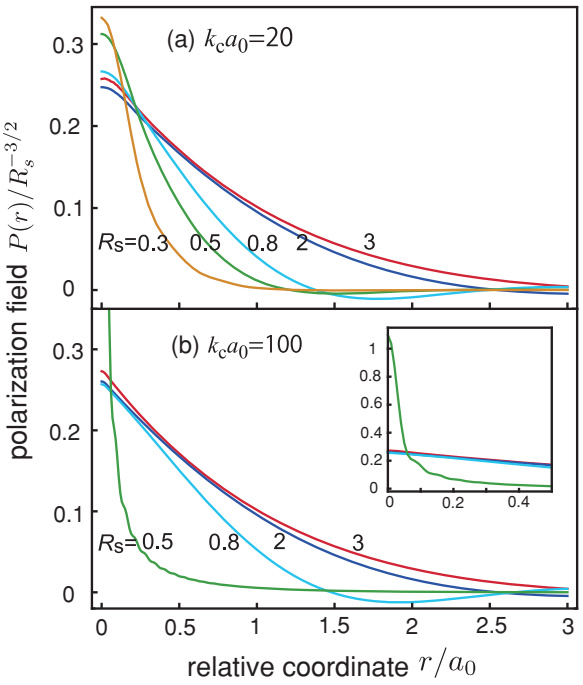

FIG. 14. (Color online) Real-space profiles of e-h wave function $P(r)/R_s^{-3/2}$ for 3D systems: (a) $R_s = 3, 2, 0.8, 0.5$, and 0.3 with $k_c a_0 = 20$ and (b) $R_s = 3, 2, 0.8$, and 0.5 with $k_c a_0 = 100$. The inset shows a magnified view of the region $r/a_0 < 0.5$. We set $\tilde{g} = 0.1$ and $d = 3$ for both graphs.

low-density regime of the phase diagrams where the polariton solutions represent the ground states are the same as those shown in Fig. 10 (for 3D systems with small $k_c = 20$). The gray area in the high-density regime indicates that the photon solutions represent the ground states. We can clearly see that the gray area widens for large k_c and small d. This implies that the photon solution becomes more stable for large cutoff owing to the enhancement of the photon-mediated attraction, as discussed in Sec. V C. Moreover, the photon solution becomes more stable for small d because the photon-mediated interaction increases as d decreases. This can be understood by considering the analogy of the enhancement of two-particle interactions by a Feshbach resonance in fermionic neutral atomic gases.[35,36] We will discuss the photon-mediated interaction in the next subsection.

Finally, note that the gray area (which corresponds to the ground states of the photon solution) is not observed for realistic values of k_c in the case of 2D systems because the cutoff effect is weaker than that in 3D systems.

C. Wave function of e-h pairs

To evaluate the difference between the polariton solution and the photon solution, we plot the wave function of an e-h pair $P(r) = (1/V)\sum_k \langle e_k h_{-k}\rangle \exp(ikr)$ as a function of the relative coordinates r between an electron and a hole, as shown in Fig. 14. The plots are obtained at various densities (R_s) for $d = 3$ and $k_c a_0 = 20$ [Fig. 14(a)] and for $d = 3$ and $k_c a_0 = 100$ [Fig. 14(b)]. In the former figure, the wave function changes its shape and narrows gradually with increasing density as compared to the wave function of the $1s$ exciton, indicating that the parameter used is in the regime where all the expected changes in the ground state are crossovers. The width a_0 is determined by the Coulomb attraction in the exciton BEC regime, and it is modified by the electric-dipole interaction for $R_s < R_s^*$, where the photonic characteristics are observed. The change in the binding force is seen more clearly in Fig. 14(b). The wave function gradually narrows as R_s decreases from 3 to 0.8, and it shows a sharp peak at $r = 0$ for $R_s \lesssim 0.7$, i.e., in the photonic BEC regime. Clearly, the width is determined by a new length scale and not by a_0, which indicates that the mechanism of e-h pairing is completely different from that in the case of dilute excitons. We find that the photon solution satisfies the conditions $v_k \ll 1$, $u_k \to 1$, and $\tilde{\lambda} \neq 0$. Therefore, the variational equation for the e-h wave function $P(r)$ reduces to

$$\left(-\frac{\hbar^2\nabla^2}{2m_r} - \frac{4\pi e^2}{\epsilon^*}\frac{1}{|r|}\right) P(r) - g\lambda\tilde{\delta}(r) = \mu P(r), \quad (16)$$

where $\tilde{\delta}(r)[= (1/V)\sum_{|k|<k_c} \exp(ikr)]$ is localized at $r = 0$ with a width of $\sim 1/k_c$ and becomes a δ function if $k_c = \infty$. Since the third term on the left side can be rewritten as $-\frac{g^2 V}{2(d-\mu)}\tilde{\delta}(r)P(r)$, we see that the photon field induces an attractive δ potential mediated by photons.[25] When considering two or three dimensions, the lowest bound-state energy of the real δ potential becomes $-\infty$. However, a momentum cutoff is introduced at this point; hence, the bound-state energy remains finite. The energy is estimated as $\varepsilon/\varepsilon_0 \sim d - \frac{3\pi}{8}\tilde{g}^2 k_c a_0$ using some approximations and the conditions $v_k \ll 1$, $\Omega \to -\infty$, and $R_s^{3/2}|\zeta/\Omega| \lesssim 1$ (the photon solution satisfies these conditions). We can conclude that the first-order transition occurs when the bound-state energy owing to the short-range attraction falls below the energy of the polariton solution. The solution to Eq. (16) for large k_c is

$$P(r) = \tilde{g}\tilde{\lambda}\left(\sum_{n=1}^{\infty}\frac{\varphi_{ns}^{b*}(0)\varphi_{ns}^{b}(r)}{(E_{ns}^{b}-\mu)/\varepsilon_0} + \sum_{|k|<k_c}\frac{\varphi_k^{s*}(0)\varphi_k^{s}(r)}{(E_k^{s}-\mu)/\varepsilon_0}\right), \quad (17)$$

where φ_{ns}^b and E_{ns}^b (φ_k^s and E_k^s) are the wave functions and the energy of the ns-exciton bound state (scattering state with momentum k), respectively. As discussed above, the chemical potential has an upper limit, i.e., $\mu/\varepsilon < d$. For a large momentum, the main contribution to $P(r)$ comes from the scattering states with $P(k) \propto k^{-2}$, and the tail of $P(k)$ is longer in the photonic regime as compared to the case of the dilute limit of $1s$ excitons [$P(k) \propto k^{-4}$]. This directly leads to the narrowing of $P(r)$. This type of strong light-matter coupling effect in a microcavity has been discussed in the literature,[37,38] wherein a similar conclusion is drawn that the effective Bohr radius of an e-h pair is reduced in the photonic branch of an exciton polariton. In our study, too, we found e-h pairs with a small radius in the photonic regime. However, the treatment of an exciton polariton by Khurgin and Citrin is different from ours; they determined the wave function of an e-h pair by solving a one-body problem in the presence of a cavity field while the carrier population, and thus the effect of Pauli blocking, was neglected. However, the physics is the same: the effective Bohr radius is reduced when the photon-mediated attraction plays a role. The difference is that the chemical potential is self-consistently determined by taking into account the

minimization of the total energy in the *e-h*-photon many-body systems in our calculation. Therefore, the change in the *e-h* wave function can be evaluated even in the case of a large carrier density.

Finally, in this subsection, we refer to the difference due to the dimensionality. The main contribution to $P(r=0)$ comes from *e-h* pairs $\langle e_k h_{-k}\rangle \propto k^{-2}$ for $k \gg 1/a_0$ in the photonic regime. After summation over high momentum states in Eq. (17), we have $P(0) \propto \log(\kappa_c)$ in 2D systems and $\propto \kappa_c$ in 3D systems. This indicates that the photon-mediated attraction is stronger in 3D systems than in 2D systems. In fact, the large cutoff effect is very weak in 2D systems compared to 3D systems, and the first-order transition is not observed unless the cutoff parameter is chosen to be unrealistically large.

VI. CONCLUSIONS

The mean-field ground states of microcavity polaritons are determined by adopting a variational approach.[28] The ground state changes from excitonic to photonic as a function of the excitation density and detuning parameter. The detuning parameter determines how the excitonic excitation becomes photonic when the density is increased. Laserlike behaviors are found for large detunings: a clear onset density is found in the photonic fraction where the carrier density starts to saturate when the detuning parameter is large. On the other hand, for small detunings, no clear onset is found.

Microscopic quantities such as electronic distribution function, wave functions of *e-h* pairs, and quasiparticle energy spectra are also determined and are found to be characterized in each regime of the phase diagram. In particular, in the photonic regime, *e-h* pairs are shown to be bound within a small radius because of photon-mediated δ attraction. The polariton condensates are shown to have similarities with the conventional lasers in terms of input-output curves and the hole-burning feature when the photon level is chosen to be excessively greater than the exciton level. The input-output curves with a smooth onset smoothly approach those with a sharp onset as a function of the detuning parameter.

Finally, we discuss the strong binding of an *e-h* pair, which is expected in the photonic regime for a large cutoff parameter. As noted above, the photon-mediated short-range attraction results in the strong binding between the *e-h* pairs with a small radius, which is determined by the inverse of the cutoff momentum k_c. Since the radius is of the same order as the lattice constant $\sim 1/k_c$, an *e-h* pair should be identified as a Frenkel exciton; this is beyond the scope of our model, which employs the effective-mass approximation. This indicates the need for other models to treat excitons with a small radius, such as the Dicke model.[22,23]

Moreover, in previous experiments,[12] normal lasing (kinetic regime) has been observed at high density before the system enters the photonic BEC regime for the following reasons: carrier heating[12] or shortening of the lifetime of polaritons in the photonic regime.[16] However, if excitation with quantum degeneracy is achieved up to sufficiently high density (possible in the future), a photonic BEC can be observed and the optical spectrum will be clearly different from that of lasers. As found in this study, the electron distribution function $f_e(k) = v_k^2$ forms a plateau at $f_e \approx 0.5$, spread over the k space.[22,33] No such feature is expected in normal lasing; instead, a dip in f_e at a momentum corresponding to the laser frequency is found (spectral hole burning[17]). In laser systems, spectral hole burning is experimentally accessible, e.g., small change in the gain spectrum at the laser frequency.[39] If similar experiments are carried out for the polariton BEC, a clear difference can be observed. The characteristic emission spectrum in the photonic BEC has also been discussed by Byrnes *et al.*,[31] wherein the possible observation of the Mollow triplet has bee mentioned.

An interesting future topic will be to clarify the difference between the photonic BEC phase in our semiconductor models and the BEC of photons in thermal equilibrium, which was found quite recently in a dye-filled microcavity laser system.[40,41]

ACKNOWLEDGMENTS

We thank Peter Littlewood, Yoshihisa Yamamoto, Tim Byrnes, Kenichi Asano, Takuma Ohashi, and Kouta Watanabe for fruitful discussions. This research is supported by KAKENHI (20104008) and also by the JSPS through its FIRST Program.

*kamide@acty.phys.sci.osaka-u.ac.jp

[1] J. Kasprzak *et al.*, Nature (London) **443**, 409 (2006).
[2] R. Balili, V. Hartwell, D. Snoke, L. Pfeiffer, and K. West, Science **316**, 1007 (2007).
[3] J. J. Baumberg *et al.*, Phys. Rev. Lett. **101**, 136409 (2008).
[4] S. A. Moskalenko and D. W. Snoke, *Bose-Einstein Condensation of Excitons and Biexcitons* (Cambridge University Press, Cambridge, 2000).
[5] L. Pitaevskii and S. Stringari, *Bose-Einstein Condensation* (Oxford Science, Oxford, 2003).
[6] S. Utsunomiya *et al.*, Nature Phys. **4**, 700 (2008).
[7] K. G. Lagoudakis *et al.*, Nature Phys. **4**, 706 (2008).
[8] A. Amo *et al.*, Nature (London) **457**, 291 (2009).
[9] A. Amo *et al.*, Nature Phys. **5**, 805 (2009).
[10] H. Deng, H. Haug, and Y. Yamamoto, Rev. Mod. Phys. **82**, 1489 (2010).
[11] L. S. Dang, D. Heger, R. André, F. Boeuf, and R. Romestain, Phys. Rev. Lett. **81**, 3920 (1998).
[12] H. Deng, G. Weihs, D. Snoke, J. Bloch, and Y. Yamamoto, Proc. Natl. Acad. Sci. U.S.A. **100**, 15318 (2003).
[13] I. Carusotto and C. Ciuti, Phys. Rev. Lett. **93**, 166401 (2004).
[14] M. H. Szymańska, J. Keeling, and P. B. Littlewood, Phys. Rev. Lett. **96**, 230602 (2006).
[15] M. Wouters and I. Carusotto, Phys. Rev. Lett. **99**, 140402 (2007).
[16] J. Kasprzak, D. D. Solnyshkov, R. André, L. S. Dang, and G. Malpuech, Phys. Rev. Lett. **101**, 146404 (2008).
[17] H. Haken, *Light: Laser Light Dynamics* (North-Holland, Amsterdam, 1986).

[18] K. Kamide and T. Ogawa, Phys. Rev. Lett. **105**, 056401 (2010).
[19] D. Bajoni, P. Senellart, E. Wertz, I. Sagnes, A. Miard, A. Lemaitre, and J. Bloch, Phys. Rev. Lett. **100**, 047401 (2008).
[20] K. Kamide and T. Ogawa, J. Phys.: Conf. Ser. **210**, 012021 (2010).
[21] K. Kamide and T. Ogawa (unpublished).
[22] P. R. Eastham and P. B. Littlewood, Phys. Rev. B **64**, 235101 (2001).
[23] J. Keeling, P. R. Eastham, M. H. Szymanska, and P. B. Littlewood, Phys. Rev. B **72**, 115320 (2005).
[24] A. S. Aleksandrov, V. F. Elesin, A. N. Kremlev, and V. P. Yakovlev, Zh. Eksp. Teor. Fiz. **72**, 1913 (1977) [Sov. Phys. JETP **45**, 1005 (1977)].
[25] F. M. Marchetti, B. D. Simons, and P. B. Littlewood, Phys. Rev. B **70**, 155327 (2004).
[26] F. M. Marchetti, M. H. Szymanska, P. R. Eastham, B. D. Simons, and P. B. Littlewood, Solid State Commun. **134**, 111 (2005).
[27] Y. Yamamoto, and A. Imamoglu, *Mesoscopic Quantum Optics* (Wiley, New York, 1999).
[28] C. Comte and P. Nozieres, J. Phys. (Paris) **43**, 1069 (1982); P. Nozieres and C. Comte, *ibid*. **43**, 1083 (1982).
[29] P. R. Eastham and P. B. Littlewood, Solid State Commun. **116**, 357 (2000).
[30] A. A. Abrikosov, L. P. Gorkov, and I. E. Dzyaloshinskii, *Methods of Quantum Field Theory in Statistical Physics* (Pergamon, New York, 1975).
[31] T. Byrnes, T. Horikiri, N. Ishida, and Y. Yamamoto, Phys. Rev. Lett. **105**, 186402 (2010).
[32] R_s^* is defined by the density above which the photonic fraction becomes larger than 20%. At low density ($R_s > R_s^*$), the boundary between exciton BEC and e-h BCS is given by $R_s = 1$. We defined "polariton BEC" as the density region where the photonic fraction is larger than 20% and less than 80%. If the fraction is larger than 80%, the BEC is thought to be photonlike, and the corresponding regime is defined as "photonic BEC."
[33] R. H. Dicke, Phys. Rev. **93**, 99 (1954).
[34] V. N. Popov, *Functional Integrals and Collective Excitations* (Cambridge University Press, Cambridge, 1987).
[35] C. A. Regal, M. Greiner, and D. S. Jin, Phys. Rev. Lett. **92**, 040403 (2004).
[36] M. Holland, S. J. J. M. F. Kokkelmans, M. L. Chiofalo, and R. Walser, Phys. Rev. Lett. **87**, 120406 (2001).
[37] J. B. Khurgin, Solid State Commun. **117**, 307 (2001).
[38] D. S. Citrin and J. B. Khurgin, Phys. Rev. B **68**, 205325 (2003).
[39] R. Frankenberger and R. Schimpe, Appl. Phys. Lett. **57**, 2520 (1990).
[40] J. Klaers, J. Schmitt, F. Vewinger, and M. Weitz, Nature (London) **468**, 545 (2010).
[41] J. Klaers, F. Vewinger, and M. Weitz, Nature Phys. **6**, 512 (2010).